An exact solution for a steady, flow-line marine ice sheet

Ed Bueler

Department of Mathematics and Statistics and Geophysical Institute, University of Alaska Fairbanks, USA
E-mail: elbueler@alaska.edu

ABSTRACT. In 1955 G. Bodvardsson published a flow-line exact solution which, though this seems not to have been recognized before, is an exact solution to the steady form of the simultaneous stress balance and mass continuity equations widely-used in numerical models of marine ice sheets. Bodvardsson's solution, which has parabolic ice thickness and constant vertically-integrated longitudinal stress, solves the steady shallow shelf approximation on a flat bed. It has elevation-dependent mass balance and, in the interpretation given here, position-dependent ice hardness. By connecting Bodvardsson's solution to the van der Veen (1983) solution for floating ice, we construct an exact solution to the "rapid-sliding" marine ice sheet problem, continuously across the grounding line. We exploit this exact solution to examine the accuracy of two numerical methods, one grid-free and the other based on a fixed, equally-spaced grid.

INTRODUCTION

Early[1] theoretical glaciology created two fundamentally-different parabolic profiles as the shapes of steady flow-line ice sheets lying on flat beds, as in Figure 1. One was the profile of an ice sheet with perfectly-plasticity (Orowan, 1949; Nye, 1952) and the other the profile for a sliding "plug" flow investigated by Bodvardsson (1955). These global views of free surface flows in glaciology focus on different aspects of the problem and they come to rather different conclusions. Up to scaling, one is of the form $x = 1 - y^2$ (Orowan-Nye) and the other is of the form $y = 1 - x^2$ (Bodvardsson). The former perfect-plasticity solution has a central peak at the highest point of the ice sheet, and a margin with unbounded surface gradient. The latter plug flow solution has a smooth dome and a finite-slope, wedge-shaped margin.

This paper shows how to combine Bodvardsson's solution with the well-known exact solution for an ice shelf (van der Veen, 1983, 2013) to generate the exact solution for a flowline, steady marine ice sheet shown in Figure 2. This exact solution simultaneously solves the steady mass continuity equation and the so-called shallow shelf approximation ("SSA"; Weis and others, 1999) stress balance. It is an exact solution of the steady form of the rapidly-sliding marine ice sheet case (Schoof, 2007), the model also addressed by the MISMIP intercomparison (Pattyn and others, 2012).

After presenting the model equations and constructing the exact solution in the next two sections, respectively, we examine errors made by two different numerical methods. Though the most significant result in this work is the identification of the exact solution itself, we also observe, through linearization of the equations around the exact solution, that the grounding line generates a strong, and now precisely measurable, numerical stiffness constrast.

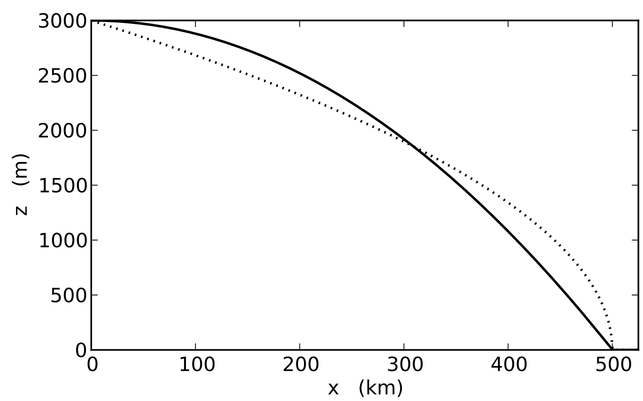

Fig. 1. The parabolas by Orowan and Nye (1949, 1952; dotted) and by Bodvardsson (1955; solid) for steady, flowline ice sheets on flat beds. A dome thickness of $H_0 = 3000$ m and a length of $L_0 = 500$ km are chosen for concreteness.

CONTINUUM MODEL

Model equations

Our model equations describe the steady-state, flat bed form of the flowline, rapid-sliding model of Schoof (2007; equations (2.1)–(2.5)). We restrict to the linear sliding case, but with a nonconstant sliding coefficient. The primary unknowns in these equations are the ice thickness $H(x)$, velocity $u(x)$, and vertically-integrated longitudinal stress $T(x)$ (Schoof, 2006),

[1] Draft date *April 2, 2014*.

where x is the flowline distance. Using other notation from Table 1, the equations are

$$(uH)_x - M = 0, \tag{1}$$

$$T_x - \beta u - \rho g H h_x = 0, \tag{2}$$

$$T = 2BH|u_x|^{\frac{1}{n}-1}u_x. \tag{3}$$

Here the subscript x denotes the derivative and

$$h = \begin{cases} H + b, & \rho H \geq \rho_w(z_o - b) \\ \omega H + z_o, & \rho H < \rho_w(z_o - b) \end{cases}, \tag{4}$$

$$\beta = \begin{cases} k\rho g H, & \rho H \geq \rho_w(z_o - b) \\ 0, & \rho H < \rho_w(z_o - b) \end{cases}, \tag{5}$$

are the surface elevation and sliding coefficient, respectively.

Equations (1)–(5) apply on an interval $0 < x < x_c$ where x_c is the floating calving-front. The grounded ice rests on flat bedrock at elevation b, a constant in this context. Note that $M(x)$ combines the surface and basal mass balance, while $B(x)$ is the ice hardness, and that these functions may depend on location x. In grounded ice the basal shear stress satisfies $\tau_b = -\beta u$ (MacAyeal, 1989), but we have scaled the coefficient with the ice overburden pressure so that $\beta = k\rho g H$ (Bodvardsson, 1955). The "Archimedean factor" $\omega = 1 - \rho/\rho_w$ relates surface elevation to thickness in floating ice. Note z_o is the elevation of the ocean surface.

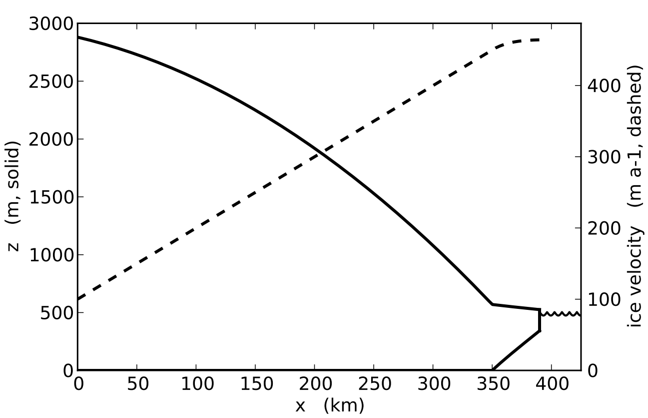

Fig. 2. The geometry (solid) and velocity (dashed) of an exact solution of the simultaneous steady mass continuity and SSA stress balance equations for a marine ice sheet. The solution is Bodvardsson's when grounded and van der Veen's when floating.

Equations (1) and (2) are the mass-continuity and SSA stress balance equations, respectively, while (3) defines T. Equation (4) says that the ice surface $z = h$ is at elevation $H + b$ when the ice is grounded, and otherwise the ice surface $z = h$ is found from the Archimedean principle. Likewise equation (5) gives the scaled form of the basal shear stress for grounded ice; it is zero for floating ice. We must solve for the location of the grounding line $x = x_g$, but at it we know $\rho H(x_g) = \rho_w(z_o - b)$.

For the exact and numerical solutions in this paper, equations (1)–(5) are augmented by boundary conditions:

$$u(0) = u_a > 0, \quad H(0) = H_a > 0, \tag{6}$$

$$T(x_c) = \frac{1}{2}\omega\rho g H(x_c)^2, \tag{7}$$

$$H, u, T \quad \text{continuous at } x = x_g. \tag{8}$$

Here $x = 0$ is an upstream location where Dirichlet boundary conditions are applied (equation (6)), while at the calving front $x = x_c$ we have the standard hydrostatic pressure "imbalance" condition (7) (Schoof, 2007). Facts (8) at x_g may be regarded as a regularity requirement, and not strictly a boundary condition; see below.

On well-posedness and the grounding line

Given data $B(x)$, b, $k > 0$, $M(x)$, $x_c > 0$, z_o, along with physical constants g, n, ρ, ρ_w, we expect the problem consisting of equations (1)–(8) to be well-posed. To our knowledge this has not been proved, nor do we attempt to prove it. It is, however, worth considering the smoothness (regularity) of the solution to (1)–(7), including what hypotheses would lead to satisfying (8) at the free (unknown) location x_g in the interior of the domain.

Indeed, suppose that, for physical reasons, the mass balance $M(x)$ and ice hardness $B(x)$ are bounded, and further that $B(x)$ is bounded below by a positive constant. From integrating M, equation (1) implies that the flux $q = uH$ is absolutely-continuous and thus bounded. If there is a positive lower bound on thickness H, then we can conclude that the magnitude of u is bounded because $u = q/H$. If the magnitude of the driving stress $-\rho g H h_x$ is bounded then equation (2) implies T is absolutely-continuous. By equation (3) this implies u has a bounded and integrable derivative, and thus that u is also absolutely-continuous. From these facts we could then return to the flux and write $H = q/u$ which shows H is absolutely-continuous away from locations where $u = 0$ (e.g. divides). In summary, assuming *(i)* that an integrable solution (H, u, T) to (1)–(7) exists, *(ii)* that the functions M, B are bounded and integrable, *(iii)* that B is bounded below by a positive constant, *(iv)* that a positive lower bound on thickness exists, and *(v)* that an upper bound on the magnitude of the driving stress exists, then we can regard conditions (8), giving continuity at the grounding line, as properties of the solution instead of as part of the "imposed" problem statement.

Table 1. Notation and SI units. Values of physical constants.

Symbol	Description	Units
B	ice hardness; $= A^{-1/n}$	$\mathrm{Pa\,s^{1/3}}$
b	bedrock elevation	m
β	sliding coefficient	$\mathrm{Pa\,s\,m^{-1}}$
g	acceleration of gravity	$9.81\ \mathrm{m\,s^{-2}}$
H	ice thickness	m
h	ice surface elevation	m
k	pressure-scaled sliding coefficient	$\mathrm{s\,m^{-1}}$
M	mass balance	$\mathrm{m\,s^{-1}}$
n	Glen exponent in ice flow law	3
ρ	density of ice	$910\ \mathrm{kg\,m^{-3}}$
ρ_w	density of sea water	$1028\ \mathrm{kg\,m^{-3}}$
T	z-integrated longitudinal stress	$\mathrm{Pa\,m}$
τ_b	basal shear stress applied to ice	Pa
u	horizontal velocity	$\mathrm{m\,s^{-1}}$
(x, z)	flow-line cartesian coordinates	m
x_g	grounding line	m
x_c	calving front	m
z_o	ocean surface elevation	m
ω	Archimedean factor; $= 1 - \rho/\rho_w$	0.115

EXACT SOLUTION

Bodvardsson's parabola

Bodvardsson (1955) built, based on minimal existing literature, a rigorous theory of the flow of glaciers and ice sheets. His test case was Brúarjökull, a glacier on the northern margin of Vatnajökull in Iceland. It flows over a smooth bed for 20 km, from a location where its thickness is 600 m, to a zero thickness margin. This glacier is entirely grounded. He shows that a good fit to measured surface elevations can be made using his model.

He initially states an equation for the ice sheet surface elevation which has both vertical-plane shear and longitudinal stress within the ice. However, he says this equation "is quite tedious and very difficult to handle especially because of the [shear] term in the parentheses. It is therefore fortunate that [the shear] term appears to be small compared to the [basal sliding] term." Then he drops the shear term and writes an equation in which driving stress is balanced entirely by sliding resistance. He solves and analyzes this plug flow model, which we now detail.

For basal resistance he chooses a coefficient which scales with the overburden pressure, so that the basal shear stress is

$$\tau_b = -k\rho g H u \tag{9}$$

He then writes the ice flux as $uH = -(H/k)H_x$, or equivalently the ice velocity as

$$u = -\frac{1}{k}H_x. \tag{10}$$

As is perhaps best-known about Bodvardsson's work, he chooses the surface mass balance to be

$$M = a(H - H_{ela}) \tag{11}$$

for a mass balance gradient $a > 0$ and equilibrium-line altitude H_{ela}. Combining these equations yields (Bodvardsson, 1955, equation (17))

$$a(H - H_{ela}) + (k^{-1}HH_x)_x = 0 \tag{12}$$

for the thickness. His solution to this equation is (Bodvardsson, 1955, equivalent equations (18) and (23))

$$H(x) = H_0(1 - (x/L_0)^2) \tag{13}$$

where $H_0 = 1.5H_{ela}$ and $akL_0^2 = 9H_{ela}$ (Bodvardsson, 1955, equation (24)).

Despite its simplicity, equation (13) is an exact solution to equation (12), with boundary condition $H(0) = H_0$, as the reader may verify. Formula (13) defines the solid parabola shown in Figure 1. Bodvardsson does not offer a reason why there should be such a simple quadratic solution. In fact, his solution even seems to be a new result for a narrow class of nonlinear second-order ODEs; see Appendix A.

Bodvardsson explicitly considers solution (13) as solving a free boundary problem, in the sense that the single boundary condition $H(0) = H_0$ applied to the equation (12) determines the quadratic solution (13); see Appendix A. Thus solving (12) with one boundary condition generates a value L_0 from the hypothesis that the flux and the thickness at $x = L_0$ are both zero.

The Bodvardsson (1955) solution for a grounded glacier was apparently first cited by Weertman (1961). Weertman decided that the physics chosen by Bodvardsson should be replaced by a shear deformation model more like the shallow ice approximation, though he allowed sliding as well. This replacement seems to have influenced readers from then on.

The surface balance parameterization (11) reappears in Weertman (1961), among many other places. It realistically parameterizes a potential climatic instability, which was Bodvardsson's, Weertman's, and most readers', major interest. We are, however, interested now in Bodvardsson's solution to the ice flow equations themselves.

An SSA re-interpretation

One can observe that (13) exactly solves a combination of the steady flow-line mass-continuity equation (1) and the SSA stress balance equation (2), but with contrived ("manufactured") ice softness. In fact, suppose we look for solutions of (1) and (2) with constant vertically-integrated longitudinal stress, $T_x \equiv 0$. In that case equation (2) and the scaling (9) implies Bodvardsson's formula for the velocity, namely equation (10). Furthermore, equations (1) and (11) then give Bodvardsson's main equation (12). That is, if *(i)* $T_x \equiv 0$, *(ii)* sliding resistance is linear and scales with overburden pressure, and *(iii)* mass balance is proportional to elevation above the equilibrium line, then we recover a simple parabolic profile for $H(x)$, namely equation (13) which is a solution to (12).

But what does the condition "$T_x \equiv 0$" imply as a relation among the modeled quantities? Given a thickness profile $H(x)$ and a strain rate profile $u_x(x)$, we may interpret "$T_x \equiv 0$" as a statement of *variable ice hardness*. Such variable hardness is physical and common to various numerical models using the SSA (Bueler and Brown, 2009, for example), so assuming such x-dependent hardness requires no conceptual extensions in the marine ice sheet modeling context. In particular, if $T = T_0$ is the constant value then equation (3) yields a formula for ice hardness,

$$B(x) = \frac{T_0}{2H|u_x|^{(1/n)-1}u_x}. \tag{14}$$

Extending the exact solution to floating ice

The value T_0 in (14) can be set by a downstream stress condition, just as it is in many models for flowline ice shelves (e.g. Pattyn and others, 2012; Schoof, 2007). Two well-known observations are relevant: *(i)* For floating ice with $\beta = 0$, equations (1)–(7) also have a known exact solution, specifically in the case where the mass balance M and the ice hardness B are constant (van der Veen, 1983, 2013). *(ii)* The vertically-integrated longitudinal stress T in a flowline ice shelf (i.e. one without lateral stresses) satisfies equation (7) at each location x in the shelf, that is, $T(x) = \frac{1}{2}\omega\rho g H(x)^2$, because this is a first integral of equation (2) if $\beta = 0$.

Based on these observations we can construct a marine ice sheet exact solution by extending Bodvardsson's grounded solution to the floating ice. First taking $b = 0$ as the flat bed elevation, we suppose the ocean has surface elevation $z_o > 0$, thus determining the grounding-line thickness $H(x_g) = (\rho_w/\rho)z_o$. Then from Bodvardsson's thickness solution (13) we can determine x_g. At x_g, from (10) and (13), we know $u(x_g)$ as well. For $x_g \le x \le x_c$, the floating ice shelf, we then set $M(x) = M(x_g)$ as constant from the formula (11), thus making $M(x)$ continuous across the grounding line, while at the same time allowing us to use van der Veen's construction (which is based on constant mass balance). The equation $T(x) = \frac{1}{2}\omega\rho g H(x)^2$ determines $T_o = T(x_g)$ for use in equation (14), which determines $B(x_g)$ in particular, and so then we set $B(x) = B(x_g)$ for

Table 2. Specific values of the exact solution shown in Figures 2–5; "g.l." = grounding line and "c.f." = calving front.

Symbol	Description	Units
b	bedrock elevation	0 m
H_0	thickness used in (13)	3000 m
L_0	length used in (13)	500 km
x_a	offset	100 km
z_o	ocean surface elevation	504.572 m
$H(0)$	thickness at $x = 0$	2880 m
$u(0)$	ice velocity at $x = 0$	100 $\mathrm{m\,a^{-1}}$
x_g	location of g.l.	350 km
$B(x_g)$	ice hardness at g.l.	4.614×10^8 $\mathrm{Pa\,s^{1/3}}$
$H(x_g)$	thickness at g.l.	570 m
$M(x_g)$	mass balance at g.l.	-4.290 $\mathrm{m\,a^{-1}}$
$T(x_g)$	stress at g.l.	1.665×10^8 Pa m
$u(x_g)$	ice velocity at g.l.	450 $\mathrm{m\,a^{-1}}$
x_c	location of c.f.	390 km
$H(x_c)$	thickness at c.f.	182.938 m
$T(x_c)$	stress at c.f.	0.171×10^8 Pa m
$u(x_c)$	ice velocity at c.f.	464.092 $\mathrm{m\,a^{-1}}$

$x_g \le x \le x_c$, a constant needed in van der Veen's construction.

The results of the above choices are the following formulas for an exact marine ice sheet satisfying our steady model equations (1)–(8). The velocity comes from combining the Bodvardsson (1955) and van der Veen (1983) results,

$$u(x) = \begin{cases} \frac{2H_0}{kL_0^2}(x + x_a), & 0 \le x \le x_g, \\ u_s(x), & x_g \le x \le x_c. \end{cases} \tag{15}$$

where $u_s(x)$ is defined by

$$u_s(x)^{n+1} = u(x_g)^{n+1} + \frac{C_s}{M(x_g)}\left(\left[Q_g + M(x_g)(x - x_g)\right]^{n+1} - Q_g^{n+1}\right) \tag{16}$$

$C_s = (\rho g\omega/(4B(x_g)))^n$, and $Q_g = u(x_g)H(x_g)$. Similarly the thickness is:

$$H(x) = \begin{cases} H_0\left(1 - (\frac{x+x_a}{L_0})^2\right), & 0 \le x \le x_g, \\ \frac{Q_g + M(x_g)(x - x_g)}{u_s(x)}, & x_g \le x \le x_c. \end{cases} \tag{17}$$

Formulas (15) and (17) define the continuous functions which are shown in Figure 2, using the specific values in Table 2.

From the thickness $H(x)$ and the velocity $u(x)$ we can find continuous functions $M(x)$ and $B(x)$ for the full flowline by using equations (11) and (14). These functions are shown in Figure 3. Then we can use equation (3) to find $T(x)$; this is shown in Figure 4. In Figure 4 we also show the sliding coefficient $\beta(x)$, which drops to zero discontinuously at

x_g. Finally Figure 5 shows a detail of the grounding line and floating ice in the exact solution.

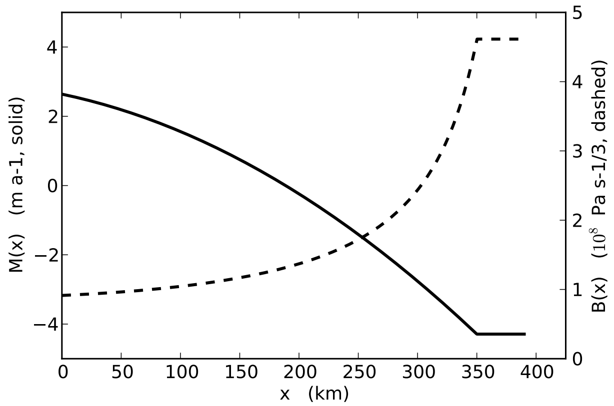

Fig. 3. The mass balance $M(x)$ (solid) and ice hardness $B(x)$ (dashed) of the exact solution.

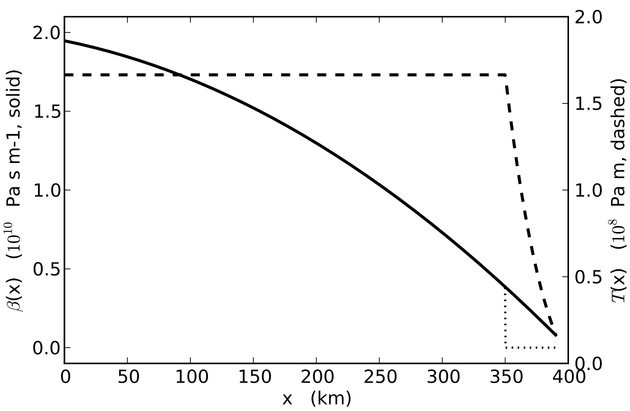

Fig. 4. The sliding coefficient $\beta(x)$ (solid) and the vertically-integrated longitudinal stress $T(x)$ (dashed) for the exact solution. The solid curve shows $\beta = k\rho g H$ on both sides of the grounding line. The actual basal resistance experienced by the shelf drops to zero at the grounding line (dotted).

Note that, because this paper is focussed on ice flow dynamics and grounding lines, we treat $M(x)$ as a predetermined field (i.e. the one shown in Figure 3). This removes the climatically-important elevation–accumulation feedback, and the associated instability, of interest to Bodvardsson (1955) and others. This feedback can be restored by using equation (11) to determine M from H.

The floating ice shelf is a relatively short 40 km; see Figures 2 and 5. To explain, note that the equilibrium line H_{ela} in Bodvardsson's (1955) solution is high on the ice sheet because of its relation to the upstream ice thickness in the construction of the exact solution (i.e. $H_{ela} = (2/3)H_0$). This in turn implies $M(x_g)$ is quite negative (equation (11); see

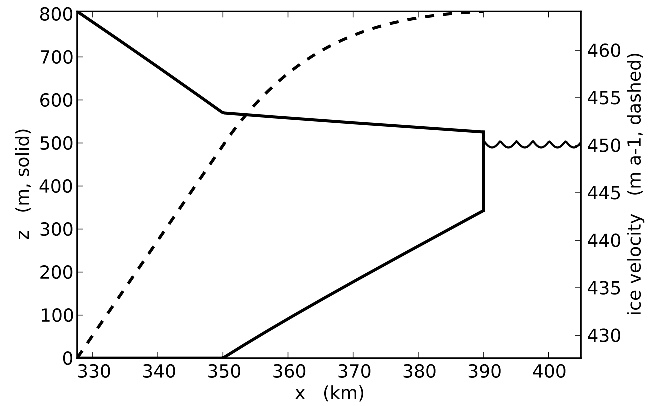

Fig. 5. Detail of Figure 2, showing the floating ice shelf geometry and velocity.

Figure 3). Because van der Veen's (1983) solution uses constant mass balance, and because we want continuity for $M(x)$, we therefore have an ice shelf experiencing rapid melting. The location of the calving front x_c must, of course, be put upstream of the location where the ice has melted away. As a result of these same factors we also see a rapid decline in the stress $T(x)$ from its constant grounded value to its small value at x_c (Figure 4 and Table 2). Though the ice shelf shown here is very wedge-like, the thickness $H(x)$ for floating ice comes from formula (17), and it is not a linear function because $u_s(x)$ is not constant on the shelf.

NUMERICAL RESULTS

Verification of a grid-free "shooting" numerical method

In our steady flowline case the model equations form a two-point boundary value problem (BVP) for ordinary differential equations (ODEs). Specifically, the three first-order ODEs (1)–(3) are subject to two boundary conditions (6) at $x = 0$ and one at $x = x_c$, the calving-front stress condition (7).

A nonlinear "shooting" method (Press and others, 1992, section 17.1) applies to this problem. We use the correct values for $u(0)$ and $H(0)$ from (6) and guess an additional value T_0 for $T(0)$. Then we use a numerical ODE initial value problem (IVP) solver to compute a solution $(\tilde{u}(x), \tilde{H}(x), \tilde{T}(x))$ from $x = 0$ to $x = x_c$. The failure of the ODE IVP solution to satisfy boundary condition (7) is a measure of the wrongness of T_0. In fact, based on (7) we define the function

$$F(T_0) = \tilde{T}(x_c) - \frac{1}{2}\omega\rho g \tilde{H}(x_c)^2 \qquad (18)$$

and then we can apply a numerical method to find the solution (root) $\hat{T}_0$ to the problem $F(T_0) = 0$. This root gives us complete initial conditions so that the ODE IVP solution also solves the two-point BVP (1)–(7).

A robust root-finding method is bisection (Press and others, 1992, section 9.1). It is guaranteed to converge if F is continuous and if an initial bracket is given (easy to find in this case). Regarding faster root-finding methods than bisection, such as Newton's method, we observe that F' may not exist because of the low regularity of the solution at the interior point $x = x_g$. However, by using our exact solution we will see clear evidence that the bisection iteration succeeds in finding the root $\hat{T}_0$ to many digits despite the uncertain smoothness of F.

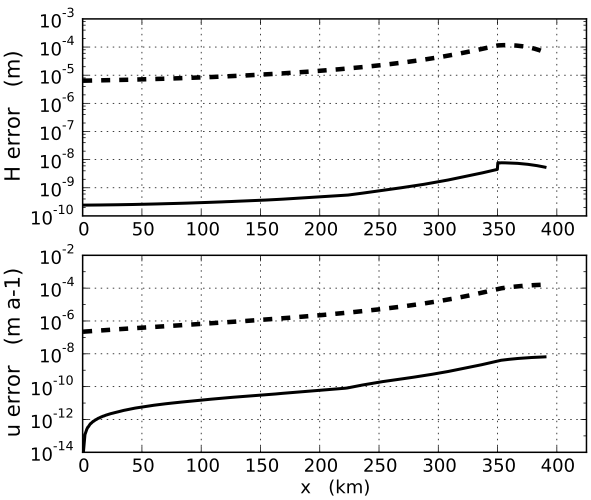

Fig. 6. Pointwise error in thickness (upper panel) and in velocity (lower panel) from an adaptive numerical ODE scheme. Both the "cheating" case (solid), where we use the exactly-correct initial value for T, and the "realistic" case (dashed), where the shooting method converges on the correct initial value for T by the bisection method, are shown.

This "shooting" method has the advantage that the advanced stepsize control mechanism of an ODE IVP solver determines the spatial grid points, so as to solve the ODEs to a desired tolerance. Thereby we avoid *a priori* choice of the grid, and in this sense the method is grid-free. In this case we use LSODA from the ODEPACK collection (Hindmarsh, 1983) because it both automatically adjusts stepsize to achieve desired tolerance and because it automatically switches method when stiffness (Press and others, 1992, section 16.6) is detected.

Of course we apply this grid-free procedure to the same problem for which we have the exact solution. Using relative tolerance 10^{-12} and absolute tolerance 10^{-14} for LSODA we get the results in Figure 6. We have show the error in two runs, one in which we have used the exactly-correct initial value T_0 ("cheating") and one in which we start with a large initial bracket on T_0 and converge on the correct calving-front boundary condition through shooting and bisection ("realistic"). In the "cheating" runs we see that the numerical error just from solving the ODE, i.e. independent of errors in boundary conditions, is quite small, perhaps the 10th or 11th digit for H and u. The much larger error seen in the "realistic" case suggests, however, that F in (18) is significantly irregular. Apparently matching the calving-front boundary condition by numerical shooting from upstream causes the loss of 4 or 5 digits of accuracy. Nonetheless, in this "realistic" case our numerical method achieves 6 or 7 digit accuracy over the whole domain, including in the immediate vicinity of the grounding line. Note that though the peak inaccuracy is near the grounding line, that error is only modestly larger than errors elsewhere.

The ODE solver also detects the grounding line as a point of transition to shorter (spatial) steps, as seen in Figure 7. More significantly, however, the grounded ice requires a stiff method while the floating ice allows a nonstiff one, according to the automatic switch mechanism in LSODA. Note that high accuracy (e.g. 6 or 7 digits) is achieved in the "realistic" case despite rather large grid spacing in the grounded ice, with large portions at 5–10 km spacing. The spacing drops to a minimum of 100 m just downstream of the grounding line at $x_g = 350$ km.

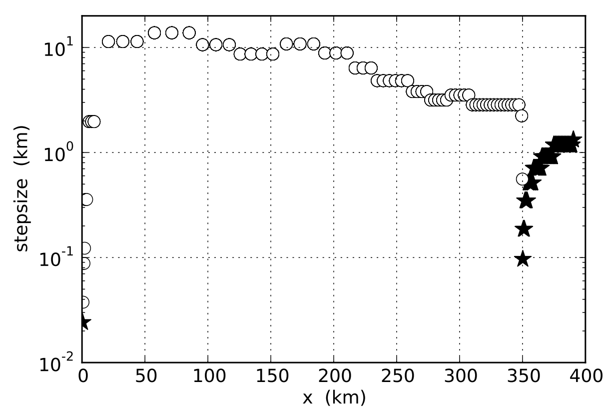

Fig. 7. The adaptive numerical ODE scheme in the "realistic" case makes steps of more than 10 km in grounded ice, but at the grounding line $x_g = 350$ km the step size is reduced to a few hundred meters. The adaptive mechanism automatically switches from stiff when grounded (circles) to non-stiff when floating (stars).

Linearization around the exact solution

The above numerical evidence shows that a distinct change in stiffness occurs at the grounding line. To analyze this we linearize the model equations around the exact solution. Denote the exact solution (u_0, H_0, T_0) and consider a small perturbation

$$u = \hat{u} + \epsilon\tilde{u}, \qquad H = \hat{H} + \epsilon\tilde{H}, \qquad T = \hat{T} + \epsilon\tilde{T}. \quad (19)$$

Denote the column vector of perturbations by $\mathbf{w} = [\tilde{u}, \tilde{H}, \tilde{T}]^T$. Assuming $u_x > 0$, equations (1)–(3) imply that, to first order in ϵ, the perturbation solves this linear ODE system in grounded ice,

$$\begin{bmatrix} \frac{2}{n} B\hat{H}(\hat{u}_x)^q & 0 & 0 \\ \hat{H} & \hat{u} & 0 \\ 0 & -\rho g\hat{H} & 1 \end{bmatrix} \mathbf{w}_x = \begin{bmatrix} 0 & -2B(\hat{u}_x)^{1/n} & 1 \\ -\hat{H}_x & -\hat{u}_x & 0 \\ -k\rho g\hat{H} & -k\rho g\hat{u} + \rho g\hat{H}_x & 0 \end{bmatrix} \mathbf{w} \quad (20)$$

where $q = \frac{1}{n} - 1$. In floating ice only the last rows differ from (20), as follows

$$\begin{bmatrix} & \dots & \\ 0 & -\omega\rho g\hat{H} & 1 \end{bmatrix} \mathbf{w}_x = \begin{bmatrix} & \dots & \\ 0 & \omega\rho g\hat{H}_x & 0 \end{bmatrix} \mathbf{w} \quad (21)$$

If we define $L(x)$ and $R(x)$ to be the left- and right-side matrices, respectively, in (20) and (21), then $\mathbf{w}$ solves

$$\mathbf{w}_x = A(x)\mathbf{w}, \quad (22)$$

where $A(x) = L(x)^{-1}R(x)$. Note that we have ordered the equations and unknowns so that $L(x)$ is lower triangular. The inverse of $L(x)$ is defined, and easy to compute, because the entries on its diagonal are nonzero.

The linear ODE system (22) is stiff if there is a large ratio of magnitudes in the eigenvalues of $A(x)$ (Press and others, 1992). Because the entries and eigenvalues of $A(x)$ are exactly computable using the exact solution values $(\hat{u}(x), \hat{H}(x), \hat{T}(x))$, we can plot, along the whole length of the flowline, the x-dependent "stiffness ratio" for $A(x)$, namely the ratio of absolute values of the real parts of the largest and smallest eigenvalues of $A(x)$. See Figure 8. This ratio is small in the nonstiff case, and it is independent of the direction of integration (i.e. upstream versus downstream). The computed ratio is by no means the last word on quantifying stiffness, which turns out to be hard problem generally (e.g. Higham and Trefethen, 1993).

We believe that the strong stiffness contrast at the grounding line is significant in explaining large near-grounding-line errors made by gridded numerical methods (Gladstone and others, 2010; Pattyn and others, 2012). This ratio drops by a factor of almost ten at the grounding line, though it is largest in the interior part of the grounded ice. It is possible

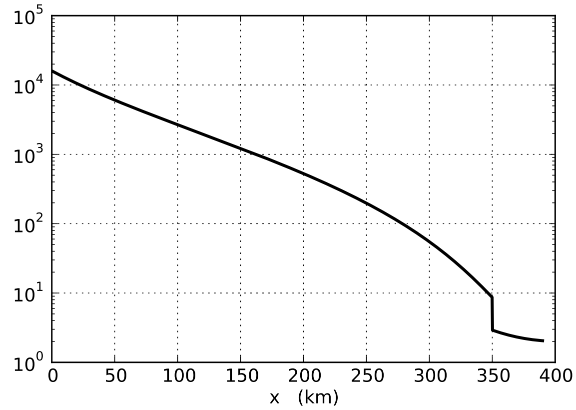

Fig. 8. Stiffness ratio for the linearized problem (22). Specifically we plot $|\mathrm{Re}(\lambda_1)|/|\mathrm{Re}(\lambda_3)|$ where λ_i are the ordered, x-dependent eigenvalues of $A(x)$ in (22).

that the benefit of modified basal stress models at the grounding line (Leguy and others, 2014, for example) can be explained as a reduction in stiffness contrast.

Verification of a fixed-grid finite difference numerical method

We also implemented an equally-spaced, second-order, finite difference scheme using Newton iteration, described in Appendix B. The new exact solution allows us to measure, for the first time in a rapidly-sliding marine ice sheet context, the errors from such a numerical scheme of the common type implemented in practical marine ice sheet models (e.g. Pollard and DeConto, 2009; Winkelmann and others, 2011).

Figure 9 shows that the maximum numerical thickness and velocity errors are observed to converge at much less than the optimal $O(\Delta x^2)$ rate under grid refinement (Morton and Mayers, 2005). This is essentially because of the low regularity (loss of smoothness) of the exact solution at the grounding line. By contrast, use of the Bodvardsson (1955) exact solution in an (entirely) grounded problem, without a grounding line, confirms that the same finite difference method gives optimal $O(\Delta x^2)$ convergence; not shown.

It is important to distinguish the errors attributable to the finite difference discretization itself from errors attributable to imperfect convergence of the nonlinear iterative solver (which is applied to solve the discretized equations). For the former type of errors we initialized the nonlinear solver with the exact solution values. These are not the exact solutions of the discretized equations but they are (obviously) close. We see converged solutions to the discretized equations down to 5 m grids. The result-

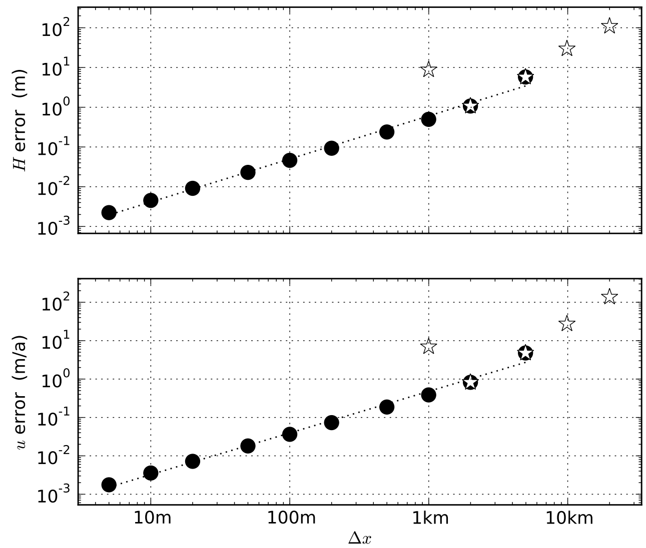

Fig. 9. Maximum errors in ice thickness (upper panel) and velocity (lower panel) on grids with spacing from 20 km down to 5 m. When initialized with the exact solution, the numerical scheme converges at a rate $\Delta x^{1.08}$ for both thickness and velocity (large dots plus dotted line). For a more realistic initial iterate the convergence rate is initially good, but at resolutions below 1 km the Newton iteration fails to converge (stars; see text).

ing thickness and velocity errors, at the millimeter and millimeter-per-year level, respectively (Figure 9), are larger than from the adaptive (grid-free) higher-order ODE method above; compare Figure 6. Nonetheless errors at this level are certainly acceptable, if they were to represent the realistic case.

However, if we use a simple "wedge" initial iterate, which has a linear thickness profile from the upstream initial condition $H(0)$ down to 300 m at the calving front, and a similar linear velocity profile increasing from $u(0)$ to 300 $\mathrm{m\,a^{-1}}$ at the calving front, then we see more realistic results which reflect the experience of ice sheet modelers addressing these equations. Here the initial iterate is relatively far from the exact solution. Difficulties arise in the global convergence behavior of the Newton solver, even though standard line search techniques are used in these computations (Kelley, 1987; Balay and others, 2011). For grids finer than 1 km the iteration for this scheme does not converge, apparently because the Jacobian matrix is not providing useful directional information as to the location of the solution of the discretized equations. In any case, our results suggest a lack of nonlinear solver robustness that we attribute to the nonsmooth, stiffness-constrasting properties of the problem near the grounding line.

Grounding line parameterizations (e.g. Gladstone and others, 2010; Feldmann and others, 2014) may act like homotopy continuation methods (Kelley, 1987) to improve global solver behavior in this case, but such considerations go beyond our scope. Alternatively, the hydrology-motivated smoothing of basal friction from Leguy and others (2014) may reduce the stiffness contrast, and this could be explored in future work. For now, no regularization of the grounding line discontinuities in the formulas for $h(x)$ and $\beta(x)$—see equations (4) and (5)—were applied in the current paper.

CONCLUSION

As noted by Bueler and others (2005), Wesseling (2001), and many other sources, verification of numerical methods is a valuable first step in effective numerical modeling of realistic flows. This is especially so in geophysical flows where validation by comparison to controlled laboratory experiments is difficult. Thus the rediscovery of an exact solution to a marine ice sheet problem is a welcome development. Even though this solution is for a steady-state and flat bed case, it provides a partial alternative to hard-to-interpret intercomparison results (Pattyn and others, 2012).

Because this solution is found in some of the first work in theoretical glaciology, we have "rescued" an early approach to sliding dynamics. The "rapid-sliding" case turns out to be one of the first dynamical situations examined (Bodvardsson, 1955), even though most early efforts at global views of ice dynamics tended toward the plastic ice (Orowan, 1949; Nye, 1952), frozen bed (Vialov, 1958), and vertical-shear dominated (Weertman, 1961) models. These came to dominate the field until recent decades.

Application of the new exact solution also reveals one feature of the marine ice sheet problem that we feel has been overlooked. Namely that there is a strong stiffness contrast, in the sense of differential equations, in the flowline case at the grounding line. This is, conceptually, in addition to the loss of smoothness seen at the grounding line. Both smoothness and stiffness must be addressed by numerical methods. Modelers should have more than grid refinement in mind as they attempt to model grounding lines correctly.

Acknowledgements and erratum

Thanks to Heinz Blatter and Helgi Björnsson for tracking down a copy of Bodvardsson (1955). Bueler and others (2005) incorrectly identify the constant accumulation SIA solution as "Bodvarsson (1955)–Vialov (1958)," but it is attributable only to Vialov. Note finally that the spelling is "Bodvarsson" in many places, but the 1955 paper has "Bodvardsson" with a "d".

REFERENCES

Balay, S. and others, 2011. PETSc Users Manual, *Tech. Rep. ANL-95/11 - Revision 3.2*, Argonne National Laboratory.

Bodvardsson, G., 1955. On the flow of ice-sheets and glaciers, *Jökull*, **5**, 1–8.

Bueler, E. and J. Brown, 2009. Shallow shelf approximation as a "sliding law" in a thermodynamically coupled ice sheet model, *J. Geophys. Res.*, **114**, f03008, doi:10.1029/2008JF001179.

Bueler, E., C. S. Lingle, J. A. Kallen-Brown, D. N. Covey and L. N. Bowman, 2005. Exact solutions and numerical verification for isothermal ice sheets, *J. Glaciol.*, **51**(173), 291–306.

Feldmann, J., T. Albrecht, C. Khroulev, F. Pattyn and A. Levermann, 2014. Resolution-dependent performance of grounding line motion in a shallow model compared to a full-Stokes model according to the MISMIP3d intercomparison, *J. Glaciol.*, **60**(220), 353–360.

Gladstone, R. M., A. J. Payne and S. L. Cornford, 2010. Parameterising the grounding line in flow-line ice sheet models, *The Cryosphere*, **4**, 605–619.

Higham, D. and L. N. Trefethen, 1993. Stiffness of ODEs, *BIT*, **33**, 285–303.

Hindmarsh, A. C, 1983. ODEPACK, A Systematized Collection of ODE Solvers, *IMACS Transactions on Scientific Computation*, **1**, 55–64, edited by Stepleman et al.

Kelley, C. T., 1987. Solving Nonlinear Equations with Newton's Method, Fundamentals of Algorithms, SIAM Press.

Leguy, G. R., X. S. Asay-Davis and W. H. Lipscomb, 2014. Parameterization of basal hydrology near grounding lines in a one-dimensional ice sheet model, *The Cryosphere Discussions*, **8**(1), 363–419.

MacAyeal, D. R., 1989. Large-scale ice flow over a viscous basal sediment: theory and application to ice stream B, Antarctica, *J. Geophys. Res.*, **94**(B4), 4071–4087.

Morton, K. W. and D. F. Mayers, 2005. Numerical Solutions of Partial Differential Equations: An Introduction, Cambridge University Press, 2nd ed.

Nye, J. F., 1952. A method of calculating the thicknesses of the ice-sheets, *Nature*, **169**(4300), 529–530.

Orowan, E., 1949. Discussion, *J. Glaciol.*, **1**(5), 231–236.

Pattyn, F., C. Schoof, L. Perichon and others, 2012. Results of the Marine Ice Sheet Model Intercomparison Project, MISMIP, *The Cryosphere*, **6**, 573–588.

Pollard, David and Robert M. DeConto, 2009. Modelling West Antarctic ice sheet growth and collapse through the past five million years, *Nature*, **458**, 329–333.

Press, W. H., S. A. Teukolsky, W. T. Vetterling and B. P. Flannery, 1992. Numerical Recipes in C: The Art of Scientific Computing, Cambridge University Press, 2nd ed.

Schoof, C., 2006. A variational approach to ice stream flow, *J. Fluid Mech.*, **556**, 227–251.

Schoof, C., 2007. Marine ice-sheet dynamics. Part 1. The case of rapid sliding, *J. Fluid Mech.*, **573**, 27–55.

van der Veen, C. J., 1983. A note on the equilibrium profile of a free floating ice shelf, IMAU Report V83-15. State University Utrecht, Utrecht.

van der Veen, C. J., 2013. Fundamentals of Glacier Dynamics, CRC Press, 2nd ed.

Vialov, S. S., 1958. Regularities of glacial shields movement and the theory of plastic viscous flow, International Association of Scientific Hydrology Publication 47 (Symposium at Chamonix 1958—Physics of the movement of ice), 266–275.

Weertman, J., 1961. Stability of ice-age ice sheets, *J. Geophys. Res.*, **66**, 3783–3792.

Weis, M., R. Greve and K. Hutter, 1999. Theory of shallow ice shelves, *Continuum Mech. Thermodyn.*, **11**(1), 15–50.

Wesseling, Pieter, 2001. Principles of Computational Fluid Dynamics, Springer-Verlag.

Winkelmann, R., M. A. Martin, M. Haseloff, T. Albrecht, E. Bueler, C. Khroulev and A. Levermann, 2011. The Potsdam Parallel Ice Sheet Model (PISM-PIK) Part 1: Model description, *The Cryosphere*, **5**, 715–726.

Appendix A: Bodvardsson's little theorem

Bodvardsson (1955) does not identify a source for the exact parabolic thickness solution to his plug flow equations, and it seems likely that he derived it from scratch. We summarize his result as the theorem that if A and B are constant then there is a unique polynomial solution $y(x)$ to the nonlinear second-order differential equation

$$(yy')' = Ay + B \qquad \text{(A1)}$$

satisfying the single boundary condition $y(0) = y_0 > 0$, subject to both an initial downslope assumption ($y'(0) \le 0$) and to the technical inequality

$$2Ay_0 + 3B \ge 0. \qquad \text{(A2)}$$

Equation (A1) is equation (17) in Bodvardsson (1955). The additional assumptions (i.e. initial downslope plus (A2)) are unstated, though he comments that there is "one and only one solution which is admittable from the physical point of view."

Here we justify this little theorem and, generally following Bodvardsson (1955), derive relations among parameters which allow a solution. The unique polynomial solution to this problem may be interpreted as solving a free boundary problem for the first positive zero $x_0 > 0$ of $y(x)$. In Bodvardsson's context $x_0 = L_0$ is the length of the glacier, the location of the margin in the "dry" case.

It is easy to see by substitution into (A1) that nontrivial solutions of degree d, i.e. of the form $y(x) = \gamma x^d + (\text{lower degree})$ with $\gamma \ne 0$, exist only if $d = 2$. In that case we seek solutions which satisfy the boundary conditions, so

$$y(x) = y_0(1 - \alpha x + \beta x^2) \qquad \text{(A3)}$$

for some $\alpha \ge 0$ and β which are to be determined from A, B; this is equation (18) in (Bodvardsson, 1955). Substitution gives the two equations

$$3y_0^2\alpha^2 = 2Ay_0 + 3B \quad \text{and} \quad 6y_0\beta = A. \qquad \text{(A4)}$$

These two relations determine α, β from A, B. The first relation explains (A2), noting $3y_0^2\alpha^2 \ge 0$ of course.

In the main text, Bodvardsson's problem relates four numbers to the unknown glacier thickness $y(x) =$

$H(x)$: the initial (upstream) ice thickness $y_0 = H_0$, an ablation gradient $a > 0$, the equilibrium-line altitude H_{ela}, and a sliding constant $k > 0$. He has $A = -ka$ and $B = kaH_{ela}$ in (A1) so the technical condition (A2) says $3H_{ela} \geq 2H_0$ after simplification. This causes the equilibrium line altitude to be relatively high on the glacier.

Appendix B: A finite difference scheme

The steady-state equations for mass continuity (1) and stress balance (2) form a coupled system that can be approximately solved by the centered, second-order finite difference scheme described here. There is no claim that this scheme is optimal, but merely that it is a reasonable choice for first evaluation, among fixed-grid methods. Because we use it to solve a steady-state problem, it may be generalized to the time-dependent case as a fully-implicit method.

We define an equally-spaced grid on the domain $[0, x_c]$. Because the boundary condition at the calving front evaluates the stress T, we put the right endpoint x_c at a "staggered" location halfway in-between grid points. If N is the number of spaces then we define $\Delta x = x_c/(N + 1/2)$ and $x_j = j\Delta x$ for $j = 0, \ldots, N + 1$. Denote the numerical approximations $H_i \approx H(x_i)$ and $u_i \approx u(x_i)$. Let $x_j^* = x_j + \Delta x/2$ be the staggered location, for $j = 0, \ldots, N$, and note $x_c = x_N^* < x_{N+1}$. Denote $B_j^* = B(x_j^*)$ and $M_j^* = M(x_j^*)$.

The mass continuity equation (1) is approximated by a second-order method centered at the staggered location. For $j = 0, \ldots, N$,

$$\frac{u_{j+1}H_{j+1} - u_jH_j}{\Delta x} - M_j^* = 0 \qquad \text{(A5)}$$

In equation (2) we avoid infinite viscosity by regularization (Schoof, 2006). Let $\epsilon = 1/x_c$ per year, i.e. a strain rate corresponding to 1 m/a velocity change over the whole domain. Also let $q = (1 - n)/n$, and define

$$F(u_l, u_r) = \left(\left(\frac{u_r - u_l}{\Delta x}\right)^2 + \epsilon^2\right)^{q/2} \frac{u_r - u_l}{\Delta x}. \qquad \text{(A6)}$$

Then we approximate the stress T at staggered points,

$$T_j^* = B_j^* \left(H_j + H_{j+1}\right) F(u_j, u_{j+1}), \qquad \text{(A7)}$$

for $j = 0, \ldots, N$. Equation (2) is approximated by

$$\frac{T_j^* - T_{j-1}^*}{\Delta x} - \beta_j u_j - \rho g H_j \frac{h_{j+1} - h_{j-1}}{2\Delta x} = 0 \qquad \text{(A8)}$$

where $\beta_j = k\rho g H_j$ if the ice is grounded at x_j (i.e. if $\rho H_j \geq \rho_w(z_o - b)$) and $\beta_j = 0$ if the ice is floating, and where $h_j = H_j + b$ if the ice is grounded and $h_j = \omega H_j + z_o$ if the ice is floating. Thus equation (A8) applies as stated both for grounded and floating ice, for $j = 1, \ldots, N$.

At this point we have $2N + 4$ scalar unknowns, namely u_j and H_j for $j = 0, \ldots, N + 1$. There are $2N + 1$ nonlinear equations in (A5) and (A8) above. The two upstream Dirichlet equations (6), namely $u_0 = u(0)$ and $H_0 = H(0)$, brings the number of equations to $2N + 3$. The following approximation of the calving front condition (7), completes the system:

$$\frac{1}{2}\omega\rho g \left(\frac{H_N + H_{N+1}}{2}\right)^2 = T_N^*, \qquad \text{(A9)}$$

where T_N^* is the approximation given in (A7).

Thus we have a system of $2N + 4$ nonlinear equations in the same number of unknowns. One can write this system abstractly as $\mathbf{F}(\mathbf{v}) = 0$. These equations are solved by Newton's method (Kelley, 1987), as implemented in the PETSc library (Balay and others, 2011). We first wrote a residual evaluation function, a C language program, which basically computes $\mathbf{F}(\mathbf{v})$ given $\mathbf{v}$. A finite-difference Jacobian matrix $J = \mathbf{F}'$ can then be computed by PETSc, and this allows us to solve systems up to size about $N = 10^3$. We also implemented an exact Jacobian using by-hand differentiation of the above formulas. For initial guesses sufficiently near the exact solution, this exact Jacobian permits solutions of the system for up to $N = 10^5$. A full analysis of the robustness and convergence rate of this Newton solver would be valuable, but it is beyond the scope of the current paper.